

JUPITER MODELS WITH IMPROVED AB INITIO HYDROGEN EOS (H-REOS.2)

N. NETTELMANN, A. BECKER, B. HOLST¹, AND R. REDMER
Institut für Physik, Universität Rostock, D-18051 Rostock, Germany
Accepted to ApJ, February 24, 2012

ABSTRACT

The amount and distribution of heavy elements in Jupiter gives indications on the process of its formation and evolution. Core mass and metallicity predictions however depend on the equations of state used, and on model assumptions. We present an improved ab initio hydrogen equation of state, H-REOS.2 and compute the internal structure and thermal evolution of Jupiter within the standard three-layer approach. The advance over our previous Jupiter models with H-REOS.1 by Nettelmann et al. (2008) is that the new models are also consistent with the observed $\gtrsim 2$ times solar heavy element abundances in Jupiter's atmosphere. Such models have a rock core mass $M_c = 0\text{--}8 M_\oplus$, total mass of heavy elements $M_Z = 28\text{--}32 M_\oplus$, a deep internal layer boundary at ≥ 4 Mbar, and a cooling time of 4.4–5.0 Gyrs when assuming homogeneous evolution. We also calculate two-layer models in the manner of Militzer et al. (2008) and find a comparable large core of $16\text{--}21 M_\oplus$, out of which $\sim 11 M_\oplus$ is helium, but a significantly higher envelope metallicity of $4.5\times$ solar. According to our preferred three-layer models, neither the characteristic frequency ($\nu_0 \sim 156 \mu\text{Hz}$) nor the normalized moment of inertia ($\lambda \sim 0.276$) are sensitive to the core mass but accurate measurements could well help to rule out some classes of models.

Subject headings: planets and satellites: individual(Jupiter) – equation of state

1. INTRODUCTION

Numerous discoveries of unusual hot Jupiters, in particular those that appear to be abnormally inflated (HD 209458b; Baraffe et al. 2003), extremely metal-rich (HAT-P-2b; Leconte et al. 2009), tidally disrupted (WASP-12b; Li et al. 2010), that are thought to have formed by gravitational instability (HR 8799b; Baruteau et al. 2011), or that even allow to study non-equilibrium chemistry in irradiated atmospheres (HD 189733b; Fortney et al. 2010), have drawn some attention away from Jupiter.

While models for exoplanets often span a variety of possible solutions due to the small number of observables characterizing the planet such as radius, mass, age, and their rather large error bars, with Jupiter we face the opposite problem that many models fail to reproduce the available observational constraints (for review, see Saumon & Guillot 2004). With the upcoming Juno mission, Jupiter will not only be back in focus, but the new data may also invalidate models that cannot cope with the expected accurate measurements for the gravity field, the moment of inertia, or the oxygen abundance in the atmosphere.

As a major source of influence on Jupiter models, Gudkova & Zharkov (1999b) identified the distribution of metals and helium onto certain layers. Saumon & Guillot (2004) demonstrated in addition the sensitivity of the Jupiter models to the equation of state (EOS) of hydrogen. In the past few years, the H EOS in the warm dense matter region where hydrogen metallizes has been improved by applying ab initio simulations (Bonev et al. 2004; Vorberger et al. 2007; Holst et al. 2008; Lorenzen et al. 2010; Morales et al. 2010b,a; Tamblyn & Bonev 2010;

Caillabet et al. 2011). The corresponding Jupiter models were consistent with the available observational constraints (Nettelmann et al. 2008, hereafter N08). However, the measured enrichment of Jupiter's atmosphere with noble gases ($\sim 2\times$ solar), and with carbon and nitrogen ($\sim 4\times$ solar) suggests that oxygen is equally abundant, leading to an atmosphere metallicity of $2\text{--}4\times$ solar. Such high values could not be obtained with the former H EOS (H-REOS.1) used in N08, which instead required solar metallicity atmospheres. This low atmospheric metallicity was confirmed by another group that used the same method of computing the high-pressure EOS data (Militzer et al. 2008). Apart from this similarity however, the Jupiter models suggested by these two groups differed from each other substantially with respect to core mass, heavy element content, and internal layering. In this paper we present new Jupiter models with $\sim 2\times$ solar metallicity atmospheres as a result of applying an improved ab initio H EOS.

In § 2 we compare the improved H EOS (H-REOS.2) with H-REOS.1 and describe our procedure of structure and evolution modeling. In § 3 we present the core mass and metallicity of our new Jupiter models and show that the difference in the Jupiter models of Militzer et al. (2008) and our group does not originate from the assumption of two or three layers (§ 3.2). We also present calculations of the moment of inertia (§ 3.3), of the characteristic frequency ν_0 of the global oscillations (§ 3.4), and of the thermal evolution (§ 3.5). We discuss Jupiter's atmospheric metallicity in § 4 and give our conclusions in § 5. Appended to this paper are descriptions of our method to calculate the entropy (Appendix A) and the moment of inertia (Appendix B).

2. METHODS

2.1. Improved H EOS

¹ CEA, DAM, DIF, F-91297 Arpajon, France

Our new hydrogen equation of state (H-REOS.2) is constructed in the same way as the former version H-REOS.1 (N08). The H EOS is assembled from different contributions at the low density range ($\rho < 0.1 \text{ g cm}^{-3}$) and the high density range ($0.2 \leq \rho \leq 9 \text{ g cm}^{-3}$). At low densities, pressure dissociation and pressure ionization do not play an important role for the EOS. For these densities, models within the chemical picture agree well with experimental data. As for H-REOS.1, we here apply the Fluid Variational Theory (FVT⁺) model (Holst et al. 2007) where ionization is neglected for temperatures below 3000 K.

In the high density range, our EOS table is obtained from finite-temperature density-functional theory molecular dynamics (FT-DFT-MD) simulations using the code VASP (Kresse & Hafner 1993, 1994; Kresse & Furthmüller 1996). There are three improvements of our new H EOS. First, due to the enormous increase in computing power we were able to perform the simulations with 256 particles in a box compared to 64 particles (Holst et al. 2008). Second, we performed them up to 50,000 K, in order to cover the interior of a warm, young Jupiter, compared to 20,000 K (Holst et al. 2008, N08). In the simulations, a quantum mechanical treatment of the molecular vibrations of the ions is not included. Thus thirdly, after completion of the simulations, we add the energy of a quantum mechanical oscillator, $u_{vib} = k_B \Theta_{vib} (0.5 + (\exp(\Theta_{vib}/T) - 1)^{-1})$, to the internal energy of each molecule and subtract its classical energy of vibration, $k_B T$. The degree of dissociation is estimated via the coordination number (see Holst et al. 2008). This contribution is non-negligible if the temperature of the system is below the vibration temperature Θ_{vib} (French & Redmer 2009). For hydrogen, we use the experimental value $\Theta_{vib} = 6338.2 \text{ K}$.

For H-REOS.1 we obtained convergence of the EOS data within 3% and estimated the overall uncertainty due to both statistical and systematic errors to be below 5%. The new ab initio data in H-REOS.2 have an uncertainty of 1% for most of the density-temperature space. They are within the uncertainty of the former data for $\rho \geq 0.3 \text{ g cm}^{-3}$ but shifted to 2% higher pressures in a T - ρ region where pressure dissociation and ionization occurs. Figure 1 shows selected isotherms. With the onset of pressure dissociation at 0.2 g cm^{-3} , the difference rises to 10%. This is a rather small density for FT-DFT-MD simulations that requires large computational effort to reach converged results. The displayed region of 5000–10000 K and 0.2 – 1 g cm^{-3} is relevant for the Jupiter adiabat. Here, the SCvH-i hydrogen EOS (Saumon et al. 1995) shows systematically higher pressures. At densities of $0.1 \leq \rho \leq 0.2 \text{ g cm}^{-3}$, the difference in pressure is a consequence of a revised interpolation between the low density regime and the data points at 0.2 g cm^{-3} . This difference is particularly pronounced for the internal energy (not shown). Along the Jupiter adiabat (Fig. 2), the revised internal energy requires higher temperatures in order to keep the entropy constant at the level defined by Jupiter’s outer boundary condition of 170 K at 1 bar (see § 2.3), and also leads to a decrease in the density at low pressures of 0.1 to 10 GPa. However, due to little mass prevalent at those pressures in Jupiter, this region does not affect our Jupiter interior models. Instead, it is

the 10–50 GPa pressure region where the lower densities of H-REOS.2 map onto the new Jupiter models.

Our EOS data tables provide the thermal EOS $P(\rho, T)$ and the caloric EOS $u(\rho, T)$, but not the specific entropy $s(\rho, T)$. In Appendix A we describe our method to derive an adiabat through a given point (P, T) .

2.2. Code improvements

Careful inspection of our code used for the calculation of Jupiter’s shape and rotation in N08 revealed that two coefficients, (one of second-order, the other one of third-order) contained errors. Their effect on Jupiter models with H-REOS.1 is twofold; *i*) the layer boundary shifts from ~ 8 to ~ 4 Mbar when the outer envelope is made to have solar metallicity; *ii*) the metallicity increases by ~ 0.02 (in absolute value) in the outer envelope and ~ 0.035 in the inner one so that the maximum total mass of metals increases from 32 to 41 M_\oplus , where the latter value was presented in N08. All other results are almost unchanged. The two errors were found by a comparison of the resulting gravitational coefficients J_{2n} , $n = 1$ –4, of linear and polytropic density Jupiter and Saturn models with analytic solutions given in Zharkov & Trubitsyn (1978), and with numerical solutions for these density distributions by T. Guillot (pers. comm. 2008). For details, see Nettelmann (2009). Another improvement of the code is the application of a Newton-Raphson scheme to find the central conditions that meet the envelope pressure and mass at the core-mantle boundary. For the current version of our code, we here introduce the label MOGROP-11 (MOdellierungsprogramm für GROsse Planeten, 2011.)

2.3. Interior structure and evolution modeling

Apart from the code improvements mentioned above, our Jupiter interior and thermal evolution models are generated by essentially the same code as introduced in N08, Nettelmann (2011), and Fortney & Nettelmann (2010), where in the latter case the code was applied to the structure and evolution calculations of Uranus and Neptune. We here recall the properties of our three-layer structure model for giant planets, review the observational constraints for the new Jupiter models, and describe the method of structure and evolution modeling.

Three-layer structure model. — A sufficient number of parameters to meet the observational constraints and boundary conditions are available if we assume a three-layer structure with two envelopes and a core. The envelopes are adiabatic, homogeneous, and consist of hydrogen, helium, and heavy elements, while the core is made of rocks. Heavy elements in the envelopes are represented by the water equation of state H₂O-REOS (French et al. 2009; N08), for helium we use He-REOS (Kietzmann et al. 2007; N08), and for rocks the formula given in Hubbard & Marley (1989). The outer envelope has a lower He abundance (Y_1) than the inner envelope (Y_2). We allow for different heavy element mass fractions in the outer (Z_1) and in the inner envelope (Z_2). The transition pressure between the envelopes P_{1-2} is a free parameter. The density and entropy are discontinuous at layer boundaries.

Observational constraints. — The models are required to meet the observational constraints for the total mass M_J , equatorial radius at the 1-bar pressure level R_J , 1-bar temperature T_1 , solid-body period of rotation ω , gravitational moments J_2, J_4, J_6 , atmospheric helium abundance Y_{atm} , and have the same He mass fraction² Y as the protosolar cloud once had. As long as the oxygen abundance below Jupiter’s water cloud deck is not measured, only the lower limit for the heavy element abundance Z_{atm} in Jupiter’s atmosphere is known. This value is $1 \times Z_\odot$ (see § 4), where Z_\odot is the protosolar cloud’s metallicity of 1.5% (Lodders 2003).

These observational constraints for the structure models can be divided into four groups depending on whether they enter the modeling procedure explicitly or need to be fitted by adjusting model parameters, and whether or not they are varied within the 1σ error bars. The first set (explicit, varied) is empty. The second set (explicit, not varied) consists of $M_J = 317.8338 M_\oplus$, $2\pi/\omega = 9\text{h } 55\text{m } 30\text{s}$ (the period of the magnetic field), the upper limit $T_1 = 170\text{ K}$, and $Y_{\text{atm}} = 0.238$. While the small uncertainties in M_J and ω would not affect the resulting models, lowering T_1 by 5 K would reduce Z_1 by $\sim 0.3 Z_\odot$ (N08), in the opposite direction to what we are aiming for. Modifying Y_{atm} by 1σ (± 0.007) changes Z_1 by about $\mp 0.3 Z_\odot$. Because Y_{atm} was measured by the Galileo entry probe at a depth where vertical convection ensures homogeneous distribution of those elements that do not form clouds (such as the noble gases) deeper inside, we set $Y_1 = Y_{\text{atm}}$. The parameters of the third group (to be fitted, not varied) are $R_J = 7.1492 \times 10^7\text{m}$ and $Y = 0.275$, whereof R_J is fitted by choosing the mean radius R_m of the equipotential surface that coincides with the 1-bar pressure level, and Y by adjusting Y_2 . We find $R_m = 10.955 R_\oplus$ and $Y_2 = 0.285\text{--}0.325$. The gravitational moments J_2, J_4 , and J_6 build the fourth group (to be fitted, varied). In particular, Z_2 is used to reproduce $J_2/10^{-6}$ within the tight observational bounds 14697(1), and Z_1 is used to adjust $J_4/10^{-6}$ to either -587 (the observed central value) or -589 (the observed upper limit) (Jacobson 2003). When J_2 and J_4 are matched, $J_6/10^{-6}$ is found to lie within 34.0 and 37.5, consistent with the observed limits (29.1–39.5; Jacobson 2003). Our computation of Jupiter’s thermal evolution makes use of the observed effective temperature $T_{\text{eff}} = 124.4 \pm 0.3\text{ K}$.

Modeling procedures. — Internal profiles of m, P, T , and ρ which depend on the radial coordinate l are obtained by numerically integrating the structure equations

$$\rho^{-1} dP/dl = -d(V + Q)/dl \quad (1)$$

and

$$dm/dl = 4\pi l^2 \rho \quad (2)$$

Equation (1) states that the force acting on a mass element with density ρ at radius l is balanced by a pressure gradient, where the force $-d(V + Q)/dl$ arises from the gravity field V and the centrifugal force with potential Q due to rigid-body rotation. Equation (2) expresses the amount of mass dm included in a spherical shell of

density ρ and thickness dl at radius l . These two ordinary, first-order differential equations are integrated inward starting at the surface $l = R_m$ with the two boundary conditions $P(R_m) = 1\text{ bar}$ and $m(R_m) = M_J$. In order to satisfy in addition the inner boundary condition $m(0) = 0$, a further parameter is needed. For this we choose the core mass M_c . Thus for given values of the observational constraints and of the transition pressure P_{1-2} , the result is one single Jupiter model, obtained in terms of the internal profile and values for Z_1, Z_2 , and M_c . To calculate the planetary shape and the gravitational moments we apply the *Theory of figures* (Zharkov & Trubitsyn 1978) up to third order as in N08 and also to fourth order. Such structures describe Jupiter at present time $t_0 = 4.56\text{ Gyr}$.

For modeling Jupiter’s thermal evolution we apply a procedure similar to that of Saumon et al. (1992). To describe Jupiter’s interior at earlier times $t < t_0$, we select a few representative structure models and generate for each of them a sequence of ~ 80 warmer interior profiles by increasing T_1 up to 800 K while $m(P_{1-2})$, M_c , and the element abundances are kept at constant values. Further models with intermediate T_1 values are then generated by interpolation. While for the structure models at present time with known $R_J(t_0)$ the core mass was chosen to ensure mass conservation, we here invert the problem to find the planet radius $R_m(t)$ for given core mass. Unlike Saumon et al. (1992), rotation is included in the approximation of spherical symmetry where the centrifugal force reduces to the zero-order term $-dQ/dl = (2/3)\omega^2 l$. We calculate the cooling curves in the usual approximation of constant angular velocity (Saumon & Guillot 2004; Fortney et al. 2011), and then also by including angular momentum conservation (Hubbard 1970), which requires just 1–3 additional iterations for a given value of T_1 , and the corresponding change in the energy of rotation, dE_{rot} . The time dt passed between profiles with different surface temperatures and hence different internal entropies is given by the equation of energy balance,

$$L_{\text{eff}} - L_{\text{eq}} = -dE_{\text{int}}/dt \quad , \quad (3)$$

where L_{eff} is the planet’s observable luminosity in the infrared and L_{eq} the luminosity the planet would have in equilibrium with the insolation. Using the *Stefan-Boltzmann law* for the energy emitted by a black body with uniform temperature, these luminosities can be used to define the commonly used temperatures $T_{\text{eff}}, T_{\text{eq}}$, and T_{int} . This way, $T_{\text{eq}}(t_0)$ is derived from the L_{eq} value given in Guillot (2005). It is set constant over time or, alternatively, varied with time according to a linear increase of the irradiation flux $F_{\text{eq}} := L_{\text{eq}}/4\pi R_m^2$, starting with $F_{\text{eq}}(0) = 0.7 F_{\text{eq}}(t_0)$ as predicted by theoretical standard models for the Sun (Bahcall & Pinsonneault 1995; Sackmann & Boothroyd 2003). Note that the solar standard evolution model predicts an increasing bolometric luminosity with time, whereas the short-wavelengths (chromospheric and coronal) emissions of the young Sun may have been up to 1000 times stronger than those of the present Sun as indicated by the measured XUV fluxes of young solar-like stars (Ribas et al. 2005). Absorbed XUV irradiation can lead to heating of and mass loss from the upper planetary atmosphere (Lammer et al. 2003) but absorption at high altitudes is not suspected to influence the energy balance of the in-

² Throughout this paper, the label Y denotes a He mass fraction with respect to the H-He subsystem.

terior (Guillot & Showman 2002). Therefore, we ignore the activity-related, time-dependent solar XUV flux in our evolution calculations for Jupiter.

The difference between the luminosities radiated away and absorbed equals the loss of the planet's intrinsic energy dE_{int} per time, see Eq. (3). In the envelope, the energy lost per mass shell simply is the heat $\delta q = T(m) ds(m)$. Guillot et al. (1995) offer a convenient closure relation by relating T_{eff} to T_1 , namely $T_1 = K T_{\text{eff}}^{1.244} g^{-0.167}$ according to the model atmosphere grid by Graboske et al. (1975), where the parameter K can be used to reproduce the observed $T_{\text{eff}}(t_0)$, and g is the surface gravity. Also like Guillot et al. (1995), we take into account the core's contribution to the planet's intrinsic luminosity. The heat loss of the core is $M_c c_v dT_{\text{core}}$, where we use $c_v = 1 \text{ J K}^{-1} \text{ g}^{-1}$ as in Guillot et al. (1995), and dT_{core} is the temperature difference of the isothermal cores of subsequent interior profiles with different T_1 values, as is $ds(m)$ the entropy difference at mass shell m between those interior profiles. Although the abundances of radioactive elements decrease exponentially with time so that the energy production from radioactive decay in rock with meteoric composition may have been an order of magnitude larger in the past than it is today, we here use the present Earth's value $L_{\text{radio}} = 2 \times 10^{13} \text{ J s}^{-1} M_{\oplus}^{-1}$ to account for this contribution. This treatment seems justified for Jupiter because we find the prolongation of the cooling time due to the core's heat loss to be 0.01 Gyr only. Thus the cooling equation reads

$$dt = - \frac{\int_{M_c}^{M_J} dm T ds + M_c c_v dT_{\text{core}} + dE_{\text{rot}}}{4\pi R^2 \sigma (T_{\text{eff}}^4 - T_{\text{eq}}^4) - L_{\text{radio}}} \quad (4)$$

After integrating Eq. (4) backward in time we obtain the cooling time τ that the particular Jupiter model needs to cool down from an arbitrarily hot initial state to the present state.

3. RESULTS

3.1. Core mass and metallicity of three-layer models

Results for the core mass, the outer envelope metallicity, and the inner envelope metallicity as functions of the depth of the layer boundary between the envelopes are shown in Fig. 3. If the layer boundary is located higher in the planet (lower transition pressures), Z_1 and Z_2 become smaller. The lighter envelopes then require a larger core mass to conserve the total mass. When Z_1 decreases down to zero, the core mass cannot grow any further. However, we do not consider models with $Z_1 < Z_{\odot}$ acceptable as this is inconsistent with Jupiter's observed atmospheric abundances. We find $Z_2 \gg Z_1$ and $M_c < 10 M_{\oplus}$ for all our acceptable three-layer models. As the gravitational moments are most sensitive to the density in the outer part of the planet at pressures of a few Mbars (J_2) or even below 1 Mbar (J_4) and increase with the local density, Z_1 must decrease when the denser inner envelope extends farther out. Otherwise, $|J_4|$ would become too large. On the other hand, as we go to higher pressures deeper inside the planet, the sensitivity of J_4 , and later also of J_2 approaches zero. Therefore, Z_1 changes only weakly with P_{1-2} for deep internal layer boundaries. However, since J_2 is adjusted by Z_2 ,

Z_2 must rise strongly with P_{1-2} in order to provide a sufficiently high mass density that is able to keep J_2 on the high level of the observed value. With rising metallicity the envelope becomes denser, so the core mass must decrease. When $M_c = 0$ is reached, the layer boundary is as deep as it can be, and Z_1 adopts a maximum value. For models with H-REOS.1, this maximum is $1.0 Z_{\odot}$ if $J_4/10^{-6}$ is adjusted to 587, and $1.5 Z_{\odot}$ if $J_4/10^{-6}$ is adjusted to 589. For models with our improved H EOS, this maximum is $2.5 Z_{\odot}$ ($J_4/10^{-6} = 587$) and $2.7 Z_{\odot}$ ($J_4/10^{-6} = 589$), respectively. This enhancement in Z_1 arises from the $\sim 2\%$ higher pressures at given hydrogen mass density (Fig. 1), implying $\sim 2\%$ lower hydrogen mass density at given pressure. The lower partial density of hydrogen in the mixture requires to be compensated for by a similar amount of metals.

Including 4th order coefficients to the calculations of Jupiter's shape and rotation systematically shifts the solutions to $\sim 0.8 Z_{\odot}$ lower outer envelope metallicities, inducing an additional uncertainty on Z_1 that is of the same size as the error bars of single observables such as T_1 and J_4 , see below. For M_c and Z_2 , the inclusion of higher-order terms has an even bigger effect than the improvement in the H EOS. Obviously, a convergence check of the solution with increasing order of the theory is highly important but beyond the scope of this paper. The accuracy of our current computer code is insufficient to reliably study the effect of higher than 4th order coefficients. From preliminary calculations, solutions with 5th order coefficients are found to lie between those of 3rd and 4th order.

Figure 3 also shows the observed element abundances in Jupiter's atmosphere. Assuming that O is equally enriched as C, these abundances indicate an average enrichment of 2 (noble gases) to 4 (C,N,O). Taking $2\times$ solar as the lower limit for Z_1 , models with $P_{1-2} < 4$ Mbar drop out of the realm of acceptable models, reducing the upper limit for the core mass down to $8 M_{\oplus}$. The total mass of metals is $M_Z = 29\text{--}32 M_{\oplus}$.

As representatives for our acceptable models we recommend models J11-4a and J11-8a, highlighted in Fig. 3. Model J11-4a is the one with the outermost possible layer boundary, i.e. at 4 Mbar. Model J11-8a has $P_{1-2} = 8$ Mbar for which Z_1 is $\geq 2Z_{\odot}$ for all of the above considered uncertainties. A machine-readable table for model J11-4a is provided as supplemental material, see Table 1. For these two models we also vary Y , Y_1 , T_1 , and J_4 within their $1\text{-}\sigma$ error bars. Modifying Y by $\Delta Y = \pm 0.05$ influences Y_2 in the same direction, and thus leads to a change in Z_2 of $\mp 8\%$. Modifying Y_1 by $\Delta Y_1 = \pm 0.05$ causes a response in Z_1 of $\mp 10\%$. Similarly, a 5 K colder 1-bar level leads to a 50% decrease in Z_1 . In both cases, Z_2 consequently changes by $\pm 3\text{--}4\%$ in the opposite direction to Z_1 , and M_c changes by $\mp 2\text{--}3\%$, again opposite to Z_2 . The colder outer envelope adiabat also cools the interior, resulting in a core that is 100 K colder. The slightly denser H-He subsystem that results reduces the amount of metals in the envelope required to match J_2 , but the net effect of ΔT_1 on Z_2 remains positive. Setting $|J_4|/10^{-6}$ down to 585 lowers Z_1 by $\sim 15\%$. Clearly, the response of Z_2 (increase) and thus of M_c (decrease) in this case is stronger than in case of ΔT_1 and ΔY_1 . Including these uncertainties, the total

mass of metals changes but insignificantly to $28\text{--}32 M_{\oplus}$.

3.2. Core mass and metallicity of two-layer models

The striking difference between the Militzer et al. (2008) (hereafter M08) predictions for the core mass of Jupiter ($16 \pm 2 M_{\oplus}$) and that of our group ($0\text{--}8 M_{\oplus}$), where both groups applied similar ab initio simulations to generate the EOS data, has prompted speculations about causes for that difference (Militzer & Hubbard 2009). We here investigate how this difference relates to the modeling assumptions of *two-layer* (M08) or *three-layer* (N08, this work) structures. For that purpose we have calculated two-layer models following M08. As in M08, the homogeneous envelope has $Y_1 = 0.238$, and the missing helium to obtain an average Y of 0.275 is not explicitly accounted for but may be part of the core mass. The core is either pure rocks or rock-ice, where we switch from ice to rock at 70 Mbar. As a result, only the innermost $4 M_{\oplus}$ are rocks. Because these models do not have the degree of freedom Z_2 , we can only match either J_2 or J_4 . As in M08 we choose to match J_2 by varying the envelope metallicity Z . We apply our usual numerical procedure (see Nettelmann 2011 for details) and vary Z , starting from 0.01, until $J_2(Z)$ meets the observed value. The core mass must decrease with increasing envelope metallicity (denser envelopes) in order to ensure total mass conservation. If the number of layers assumed for the structure of the model were responsible for the different Jupiter models we would expect to obtain the same two-layer model as in M08. This is *not* the case, as illustrated in Fig. 4. While the M08 models require $4 \pm 2 M_{\oplus}$ heavy elements in the envelope to meet J_2 , corresponding to $Z = 1.0 \pm 0.5 Z_{\odot}$ for a $16 M_{\oplus}$ core, our two-layer models require $Z = 4.3 Z_{\odot}$.

This significantly larger envelope metallicity of our two-layer models enables us to make a transition to three-layer models where metals are shuffled from the outer part of the envelope to the inner part in order get $|J_4|/10^{-6}$ down to the observed value (from 611 to 587). The M08 models do not have this degree of freedom as the already low envelope metallicity would become zero long before J_4 is matched. Hence the M08 models stay at $J_4/10^{-6} = 614$ and a large core while our two-layer models can undergo a transition to three-layer models where Z_1 becomes smaller and Z_2 larger than in the homogeneous envelope case. As a consequence of large Z_2 values, the core mass decreases further. In contrast, the core mass of the two-layer models is large because this mass also contains the missing mass of helium $dM_{\text{He}} = (0.275 - 0.238)(M_J - M_c) \sim 11 M_{\oplus}$ needed for an overall abundance $Y = 0.275$. Thus the ice-rock core mass of two-layer models is about $5\text{--}10 M_{\oplus}$, just at the upper limit of our three-layer models. This estimate would also hold for the two-layer model of M08. However, we cannot reproduce their Jupiter model, the reason for which remains unexplained at the moment. We conclude that the difference between the M08 two-layer models and our three-layer models does not originate from assumptions about the number of layers, but instead is a symptom of already different models within the two-layer frame.

3.3. Moment of inertia

We have calculated the moment of inertia I as described in Appendix B. The non-dimensional form (λ)

is obtained as $\lambda = I M_J^{-1} R_m^{-2}$. For all of our three-layer models, we find an almost invariant value $\lambda = 0.27605 \pm 0.03\%$. If we ignore Jupiter's shape deformation, the resulting λ decreases by 4% down to $0.26539 \pm 0.03\%$. This is close to the predictions of 0.2629–0.2645 of Helled et al. (2011), who considered a broad set of interior models with core masses between 0 and $40 M_{\oplus}$ as allowed by the use of six-order polynomials to represent the pressure-density relation in Jupiter's envelope. From our calculations we conclude that λ is not an appropriate parameter to constrain Jupiter's core mass further. In contrast, Helled et al. (2011) found a significant variation of 0.6% over the full range of their models and still a 0.2% variation when excluding models with M_c larger than $10 M_{\oplus}$. Juno's measurement of Jupiter's λ is expected to have an accuracy of 0.2% (Helled et al. 2011), hence sufficient to distinguish between the different predictions.

3.4. Characteristic frequency

Jovian seismology has been long recognized as a unique opportunity to infer interior structure properties (Vorontsov et al. 1976). In particular, the predicted low-frequency acoustic free oscillations depend sensitively on the core mass and internal layer boundaries of theoretical Jupiter models (Gudkova & Zharkov 1999a). However, the expected small amplitudes (~ 10 cm) and Jupiter's rapid rotation make it difficult to measure acoustic modes. Recently, Gaulme et al. (2011) used the SYMPA spectrometer to detect the lowest frequency modes ($\sim 1000 \mu\text{Hz}$) of Jupiter from spatially resolved radial velocity measurements. In the approximation of low degrees l and overtones of high radial order $n \gg l$, the acoustic modes $\nu_{n,l}$ are proportional to the characteristic frequency ν_0 (also called equidistance) and are equally spaced by ν_0 for given l : $\nu_{n,l} \simeq (n + 1/2)\nu_0$. Gaulme et al. (2011) observed $\nu_0 = 155.3 \pm 2.2 \mu\text{Hz}$. The inverse of ν_0 is twice the time a sound wave needs to travel from the center to the surface (Jupiter's troposphere),

$$\nu_0 = \left[2 \int_0^{R_J} dr c_s^{-1} \right]^{-1}, \quad (5)$$

a useful parameter that interior models can easily be compared to. In Eq. 5, c_s is the adiabatic sound velocity. Gudkova & Zharkov (1999a) calculate $\nu_0 = 152\text{--}155 \mu\text{Hz}$ for SCvH-i EOS based Jupiter models with five layers and core masses of $3\text{--}10 M_{\oplus}$. Gaulme et al. (2011) obtain the same range of values for ν_0 with three-layer models of Jupiter that have a small internal He discontinuity and core masses of $0\text{--}6 M_{\oplus}$. For our three-layer models with $M_c = 0\text{--}8 M_{\oplus}$ we find $\nu_0 = 155.7\text{--}156.3 \mu\text{Hz}$. Since this range is rather narrow and slightly above that of former Jupiter models, a more accurate determination of the global mode spacing may help to rule out some Jupiter models but not constrain Jupiter's core mass further within the current uncertainty of $\sim 0\text{--}10 M_{\oplus}$.

3.5. Cooling curves

For a better comparison with published calculations of the cooling of Jupiter we first assume a constant irradiation flux and constant angular velocity over time. The latter assumption is justified by the rather small change

of the rotational energy during evolution compared to Jupiter’s intrinsic energy loss (Hubbard 1977) and the small change in planet radius over most of the contraction time scale (Guillot et al. 1995). Our H-REOS.2 based Jupiter model J11-4a has a calculated cooling time of 4.66 ± 0.04 Gyr, see Fig. 5, and model J11-8a of 4.68 ± 0.04 Gyr, where the uncertainty mostly arises from the observational error bar of T_{eff} . This result can be considered in good agreement with the age of the solar system ($\tau_{\odot} = 4.56$ Gyrs) given that none of the alternative proposed Jupiter models that rely on free-energy models for the equation of state (Saumon & Guillot 2004), such as LM-H4 (4.0 Gyr), SCvH-i (4.7 Gyr), and LM-SOCP (4.8 Gyr) gives a better agreement. On the other hand, Fortney et al. (2011) investigated the uncertainty arising from the use of the Graboske et al. (1975) model atmosphere grid for Jupiter’s evolution. If instead a self-consistent model atmosphere grid was applied as it is the common approach for exoplanets, Jupiter’s cooling time increases by ~ 0.5 Gyr. Sinking He droplets from H-He phase separation in Jupiter would also prolong the cooling time further. A process working in the opposite direction could be rising material from core erosion. During the first 500 Myr, Jupiter has shrunk from $1.4\text{--}1.5R_J$ down to $1.1R_J$ (Fig. 5). Because the initial conditions for the long-term evolution of a $1 M_J$ planet are forgotten after 0.01 Gyr (Marley et al. 2007), we consider the displayed radius evolution at young ages realistic.

In a second step, we keep the angular momentum conserved to Jupiter’s current value (within a numerical accuracy of 0.4% which gives sufficiently smooth evolution curves) and include the subsequent change of rotational energy $dE_{\text{rot}}(t)$, as also done in Hubbard (1970). Such second order effects are important for estimates of the size of the correction factors that are necessary to bring the cooling time in agreement with τ_{\odot} . It is clear that both effects (λ and dE_{rot}) will prolong the cooling time: *i*) for the same total mass, a larger planet (the young Jupiter) rotates slower, implying a weaker centrifugal force that pushes matter outward, and the consequently smaller radius will allow less energy to be radiated away from the surface; *ii*) angular momentum conservation ($L = I\omega$) then implies a lower energy of rotation $E_{\text{rot}} = 1/2 L\omega$ at young ages. The increase in E_{rot} with time must be compensated for by a reduced luminosity, implying again a longer cooling time. For model J11-4a, the first effect increases τ by 0.1 Gyr, and the second one by 0.2 Gyr, so that we find $\tau = 4.96$ Gyr. In a third step, we consider a time-dependent solar irradiation by a linear approximation of the Sun’s luminosity evolution, which is assumed to have started with 70% of the current value. We find the lower irradiation to speed up the cooling by ~ 0.6 Gyr, so that we end up with $\tau = 4.41 \pm 0.04$ Gyr. Figure 6 shows the relations between the structure parameter T_1 that determines the planet radius, $P = 2\pi/\omega$ and λ . Their evolution with time can be read from the cooling curve $T_1(t)$.

The resulting cooling times of 4.4 Gyr (linearly increasing insolation) to 5.0 Gyr (constant insolation) suggest a reasonable understanding of Jupiter’s interior and evolution, where remaining uncertainties seem to be attributable to uncertainties in the luminosity evolution of the Sun. This may be counter-intuitive as the present Sun is, by means of accurate helioseismology, far better

constrained than Jupiter. For instance, uncertainties in the sound velocity profile of the solar standard model are of the order of 0.1% only (Boothroyd & Sackmann 2003). On the other hand, non-standard solar evolution models that predict a bright and more massive young Sun (Sackmann & Boothroyd 2003) cannot completely be ruled out by observationally derived stellar mass loss rates, see Güdel (2007) for a review.

However, homogeneous, adiabatic evolution models for Saturn and Uranus that are equivalent to those presented here for Jupiter keep failing to reproduce the observed luminosities (Fortney et al. 2011), indicating that the standard three-layer model assumption may be too simplistic for some giant planets. Therefore, Leconte & Chabrier (2012) investigated the possibility of layered convection in Jupiter, where heat is transported inefficiently by diffusion across thin stable layers, separated vertically by convective cells. They determined the maximum super adiabaticity that would give density distributions in agreement with the gravity field data. The deduced presence of roughly 10^4 diffusive interfaces in Jupiter will qualitatively reduce the heat flux out of the deep interior and shorten the cooling time (Stevenson 1985). Quantitative estimates of (at least) this effect are necessary before one can conclude a reasonable understanding of Jupiter’s evolution.

4. DISCUSSION

According to our new Jupiter models with the improved H EOS (H-REOS.2), metals are enriched by a factor of at most 2.7 in the outer envelope and atmosphere. That value can be increased to 3.0 if the atmospheric He abundance is lowered by 1σ , but remains close to the lower limit of the measured C and N abundances. However, Jupiter’s atmospheric metallicity is not directly observable. What can be measured are the abundances of single chemical species from which the atomic ratios with respect to the number of H atoms can then be inferred. Such measurements have been obtained for Jupiter by remote sensing with the Voyager IR and UV spectrometers, IR spectrometry with the Earth Orbiter ISO, Galileo orbiter measurements in the near IR, the Galileo Probe Mass Spectrometer (GPMS) data, and ground-based remote sensing from IR to radio wavelengths. Among the detected species, the measured abundances of C, N, S, P, Ar, Kr, and Xe (see Fig. 3) are taken to be representative for the convective region below the 1-bar level, the outer boundary of our models, as they are not subject to non-equilibrium chemistry, cloud formation, or other processes that could significantly affect their abundance at such low altitudes (Atreya et al. 2003). Therefore, the enrichment of these elements is assumed to be representative also for those elements that are still subject to such processes, such as oxygen. The Juno orbiter, which is on route to Jupiter, is designed to measure the O abundance below the cloud level. In Fig. 7 we vary the O:H ratio and calculate the corresponding metallicity of Jupiter’s atmosphere with the help of Eq. (6),

$$Z_1 = \frac{\sum_i \mu_i (N_i:\text{H})}{\mu_{\text{H}} + \mu_{\text{He}}(\text{He}:\text{H}) + \sum_i \mu_i (N_i:\text{H})}, \quad (6)$$

where μ_i is the atomic weight of species i . By taking into account the measured abundances $N_i:\text{H}$ with their

error bars (mean, minimum, and maximum values) and including the non-detected elements {Mg, Al, Ca}, because they are abundant in the solar system, with enrichment factors of 0, 1, and $3\times$ solar, we aim to cover the uncertainty in Jupiter’s metallicity for a given O:H ratio. The unknown abundances of Mg, Al, and Ca contribute an uncertainty to Jupiter’s Z_1 of $\pm 0.2 \times Z_\odot$, and the observational error bars of the measured species contribute an additional $\pm 0.3 \times Z_\odot$.

Assuming Jupiter accreted its volatiles as a result of infall of icy planetesimals from cold, outer regions of the protosolar cloud which resembled the interstellar medium as we observe it today (Owen & Bar-Nun 1995), we would expect O:H to be similarly enriched in Jupiter as C:H (Owen et al. 1999), i.e. $\text{O:H} \geq 3\times$ solar. For this ratio we derive from Fig. 7 a minimum atmospheric metallicity of $2 Z_\odot$ that Jupiter models should satisfy. A $\sim 2.5\times$ solar metallicity (this work) is consistent with an O:H of $2\text{--}4\times$ solar. A measured O:H ratio greater than $4.5\times$ solar would not be consistent with the Jupiter models presented here. According to the uncertainties discussed above, the measured O:H ratio at the 19 bar level sets a lower limit to Jupiter’s envelope metallicity of $0.8\text{--}1.9 Z_\odot$ (based on Fig. 7).

The metallicity of the envelope is directly tied to the density of the H-He mixture for fixed (T, P) . Our models are always warmer ($T_c \sim 20,000$ K) than the M08 models ($T_c \sim 14,000$ K) implying a less dense H-He mixture that allows to add more metals compared to the M08 Jupiter adiabat. This is surprising as non-linear H-He mixing effects, which have been shown to decrease the density of the mixed phase (Vorberger et al. 2007) compared to the linear mixture that we apply, are already included in the H-He EOS of the M08 Jupiter models. Non-linear H-He mixing effects remain an appealing possibility (see N08) to enhance Z_1 in our three-layer Jupiter model calculations further.

We favor the three-layer models over the two-layer models as they allow to reproduce J_4 without invoking the hypothesis of deep-zonal winds because the penetration depth of such winds might have to be much deeper ($< 0.96 R_J$) than physically allowed in the presence of convective flow motions (Liu et al. 2008). If deep-zonal winds indeed exist and require a correction of J_4 as proposed in M08, the atmospheric metallicity of our Jupiter models would then rise up to $4.5 Z_\odot$ and the ice-rock core mass up to $12 M_\oplus$.

The three-layer model framework is amenable to additional variations. Fortney & Nettelmann (2010) modified the composition of the core by adding envelope material to the core region mimicking a diluted core. For extremely diluted cores with rock mass fraction below 20% in the central region, they found a 50% enhancement of the resulting atmospheric metallicity of Jupiter. Thus the relatively low outer envelope metallicities of our models suggest that diluted cores, possibly from core erosion, may be a better assumption for Jupiter than pure rock cores.

5. CONCLUSIONS

We have aimed to push three-layer Jupiter models with our improved H EOS (H-REOS.2) in the direction of largest possible outer envelope metallicity Z_1 . We find $Z_1 \lesssim 3.0 Z_\odot$, corresponding to an O:H enrichment fac-

tor $\lesssim 5$. However, we prefer our models with $Z_1 = 2.0\text{--}2.5 Z_\odot$, corresponding to $\text{O:H}=1\text{--}4 \text{ O:H}_{\text{solar}}$, because they do not require to push all constraints to their 1σ uncertainty limits. This increase in the envelope metal content compared to our earlier Jupiter models based on the H-REOS.1 hydrogen EOS arises from about 2% higher pressures in the $0.2\text{--}1 \text{ g cm}^{-3}$ and $5,000\text{--}10,000$ K region of the H EOS, where the ab initio simulations are challenging since dissociation and ionization occurs. The resulting Z_1 values in our Jupiter models depend on the depth of the assumed transition to a helium-rich inner envelope. The imposed constraint $Z_1 > 2 Z_\odot$ requires a transition at $P_{1-2} \geq 4$ Mbar. This threshold rises to $P_{1-2} \geq 7$ Mbar if fourth order terms in the rotational perturbation of Jupiter’s gravity field and shape are included. Future investigations of the internal structure of Jupiter, and also of Saturn, should include a convergence check of the models with respect to the treatment of rotation.

Our two-layer model calculated with our EOS and our code differs from the Militzer et al. (2008) Jupiter model. We find a larger envelope metallicity ($4.5 Z_\odot$) that enables us to switch over to a three-layer model where the envelope is divided into a metal-poor outer and a metal-rich inner part to the expense of the core mass. In a low metallicity envelope (the M08 Jupiter model), this degree of freedom does not exist. The origin of the differences between these two-layer Jupiter models remains unexplained.

For our three-layer models we calculate a cooling time of $4.4\text{--}5.0$ Gyrs, an asymptotic frequency spacing $\nu_0 = 156 \pm 0.03 \mu\text{Hz}$ for global oscillation modes, and a normalized moment of inertia $\lambda = 0.276 \pm 0.04\%$. These models are consistent with the available observational constraints. The Juno mission will be very helpful for further constraining Jupiter’s interior by measuring the deep atmospheric oxygen abundance, higher-order gravitational moments, and the moment of inertia.

The authors are grateful to the referee for the many comments and suggestions that significantly helped us to convert the initial manuscript into this paper. We acknowledge insightful discussions with J. Fortney, T. Guillot, and M. French, and thank U. Kramm for copy editing. This work was supported by the DFG RE 881/11-1, the DFG SFB 652, the North-German-Supercomputing Alliance (HLRN) and the Computing Center of the University of Rostock.

REFERENCES

- Atreya, S. K., Mahaffy, P. R., Niemann, H. B., Wong, M. H., & Owen, T. C. 2003, *Planet. Space Sci.*, 51, 105
- Bahcall, J. N., & Pinsonneault, M. H. 1995, *Rev. Mod. Phys.*, 67, 781
- Baraffe, I., Chabrier, G., Barman, T. S., Allard, F., & Hauschildt, P. 2003, *A&A*, 402, 701
- Baruteau, C., Meru, F., & Paardekooper, S.-J. 2011, *MNRAS*, 416, 1971
- Bonev, S. A., Militzer, B., & Galli, G. 2004, *Phys. Rev. B*, 69, 014101
- Boothroyd, A. I., & Sackmann, I.-J. 2003, *ApJ*, 583, 1004
- Caillabet, L., Mazevet, S., & Loubeyre, P. 2011, *Phys. Rev. B*, 83, 094101
- Fortney, J. J., Ikoma, M., Nettelmann, N., Guillot, T., & Marley, M. S. 2011, *ApJ*, 729, 32

- Fortney, J. J., & Nettelmann, N. 2010, *Space Sci. Rev.*, 152, 423
- Fortney, J. J., Shabram, M., Showman, A. P., Lian, Y., Freedman, R. S., Marley, M. S., & Lewis, N. K. 2010, *ApJ*, 709, 1396
- French, M., Mattsson, T. R., Nettelmann, N., & Redmer, R. 2009, *Phys. Rev. B*, 79, 054107
- French, M., & Redmer, R. 2009, *J. Phys.: Condens. Matter*, 21, 375101
- Gaulme, P., Schmider, F.-X., Gay, J., Guillot, T., & C., J. 2011, *A&A*
- Graboske, H. C., Pollack, J. B., Grossman, A. S., & Olness, R. T. 1975, *ApJ*, 199, 265
- Güdel, M. 2007, *Living Rev. Solar Phys.*, 4, 3
- Gudkova, T. V., & Zharkov, V. N. 1999a, *Planet. Space Sci.*, 47, 1211
- . 1999b, *Planet. Space Sci.*, 47, 1201
- Guillot, T. 2005, *Ann. Rev. Earth & Plan. Sciences*, 33, 493
- Guillot, T., Chabrier, G., Gautier, D., & Morel, P. 1995, *ApJ*, 450, 463
- Guillot, T., & Showman, A. P. 2002, *A&A*, 385, 156
- Helled, R., Anderson, J. D., Schubert, G., & Stevenson, D. S. 2011, *Icarus*, 216, 440
- Holst, B., Nettelmann, N., & Redmer, R. 2007, *Contrib. Plasma Phys.*, 47, 368
- Holst, B., Redmer, R., & Desjarlais, M. P. 2008, *Phys. Rev. B*, 77, 184201
- Hubbard, W. B. 1970, *ApJ*, 162, 687
- . 1977, *Icarus*, 30, 305
- Hubbard, W. B., & Marley, M. S. 1989, *Icarus*, 78, 102
- Jacobson, R. A. 2003, JUP230 orbit solution.
http://ssd.jpl.nasa.gov/?gravity_fields_op
- Kietzmann, A., Holst, B., Redmer, R., Desjarlais, M. P., & Mattsson, T. R. 2007, *Phys. Rev. Lett.*, 98, 190602
- Kresse, G., & Furthmüller, J. 1996, *Phys. Rev. B*, 54, 11169
- Kresse, G., & Hafner, J. 1993, *Phys. Rev. B*, 47, 558
- . 1994, *Phys. Rev. B*, 49, 14251
- Lammer, H., Selsis, F., Ribas, I., Guinan, E. F., Bauer, S. J., & Weiss, W. W. 2003, *ApJ*, 598, L121
- Leconte, J., Baraffe, I., Chabrier, G., Barman, T., & Levrard, B. 2009, *A&A*
- Leconte, J., & Chabrier, G. 2012, *A&A*, accepted
- Li, S.-L., Lin, D., Miller, N., & Fortney, J. J. 2010, *Nature*, 463, 1054
- Liu, J., Goldreich, P. M., & Stevenson, D. S. 2008, *Icarus*, 196, 653
- Lodders, K. 2003, *ApJ*, 591, 1220
- Lorenzen, W., Holst, B., & Redmer, R. 2010, *Phys. Rev. B*, 82, 195107
- Marley, M. S., Fortney, J. J., Hubickyj, O., & Bodenheimer, P. 2007, *ApJ*, 655, 541
- Militzer, B., & Hubbard, W. B. 2009, *Ap&SS*, 322, 129
- Militzer, B., Hubbard, W. B., Vorberger, J., Tamblyn, I., & Bonev, S. A. 2008, *ApJ*, 688, L45
- Morales, M. A., Pierleoni, C., & Ceperley, D. M. 2010a, *Phys. Rev. E*, 81, 021202
- Morales, M. A., Pierloni, C., Schwegler, E., & Ceperley, D. M. 2010b, *PNAS*, 102, 12799
- Nettelmann, N. 2009, PhD thesis, Universität Rostock
- . 2011, *Ap&SS*, 336, 47
- Nettelmann, N., Holst, B., Kietzmann, A., French, M., Redmer, R., & Blaschke, D. 2008, *ApJ*, 683, 1217
- Owen, T., & Bar-Nun, A. 1995, *Icarus*, 116, 215
- Owen, T., Mahaffy, P., Niemann, H. B., Atreya, S., Donahue, T., Bar-Nun, A., & de Pater, I. 1999, *Nature*, 402, 269
- Ribas, I., Guinan, E. F., Güdel, M., & Audard, M. 2005, *ApJ*, 622, 680
- Sackmann, I.-J., & Boothroyd, A. I. 2003, *ApJ*, 583, 1024
- Saumon, D., Chabrier, G., & van Horn, H. M. 1995, *ApJS*, 99, 713
- Saumon, D., & Guillot, T. 2004, *ApJ*, 609, 1170
- Saumon, D., Hubbard, W. B., Chabrier, G., & van Horn, H. M. 1992, *ApJ*, 391, 827
- Stevenson, D. S. 1985, *Icarus*, 62, 4
- Tamblyn, I., & Bonev, S. A. 2010, *Phys. Rev. Lett.*, 104, 065702
- Vorberger, J., Tamblyn, I., Militzer, B., & Bonev, S. A. 2007, *Phys. Rev. B*, 75, 024206
- Vorontsov, S. V., Zharkov, V. N., & Lubimov, V. N. 1976, *Icarus*, 27, 109
- Zharkov, V. N., & Trubitsyn, V. P. 1978, *Physics of Planetary Interiors* (Tucson, AZ: Parchart)

APPENDIX

METHOD OF CALCULATING THE ENTROPY

The functions $P(\rho, T)$ and $u(\rho, T)$ contain the full thermodynamic information. We first re-construct the free energy F and then use the Gibbs-Duhem relation to convert to entropy. It allows to derive the specific entropy $s(\rho, T)$ with an offset s_0 with respect to a reference state (ρ_0, T_0) . The offset is unknown but constant for a given reference state. First, F is derived with an unspecified offset $F_0 = F(\rho_0, T_0)$ by integration of the total differential $d(F/T)$ along some path in $\rho - T$ space. F is related to the entropy by definition, $F = U - TS$, where $U = Mu$ and $S = Ms$ are the extensive internal energy and the extensive entropy, respectively, and $M = V\rho$ is the mass contained in volume V . With the reference state (T_0, V_0) and the unknown entropy offset s_0 we can write

$$S(T, V) = \frac{U(T, V)}{T} - \left(\frac{F(T, V)}{T} - \frac{F(T_0, V_0)}{T_0} \right) + s_0 M. \quad (\text{A1})$$

The term in parenthesis in Eq. (A1) is the solution to the line integral

$$\int_{T_0, V_0}^{T, V} d \frac{F(T', V')}{T'}, \quad (\text{A2})$$

and independent of the chosen path of integration if the EOS data are thermodynamically consistent. We choose lines of constant density and of constant temperature as our path of integration. While this is a choice of convenience it has the drawback of requiring a large scale EOS in $T - \rho$ space off the planetary adiabat. With $dU = -P dV + T dS$ we have

$$\frac{d(U/T - S)}{dT} dT = -\frac{U}{T^2} dT, \quad \frac{d(U/T - S)}{dV} dV = -\frac{P}{T} dV. \quad (\text{A3})$$

After switching back to (ρ, T) -space we can write

$$\frac{1}{M} \int_{T_0, \rho_0}^{T, \rho} d \frac{F(T', \rho')}{T'} = \int_{\rho_0}^{\rho} d\rho' \frac{1}{\rho'^2} \frac{P(T_0, \rho')}{T_0} - \int_{T_0}^T dT' \frac{u(T', \rho)}{T'^2}. \quad (\text{A4})$$

After integrating the right hand side of Eq. (A4) we can numerically calculate the entropy

$$s(\rho, T) = \frac{u(T, \rho)}{T} - \frac{1}{M} \int_{T_0, \rho_0}^{T, \rho} d \frac{F(T', \rho')}{T'} + s_0. \quad (\text{A5})$$

If the underlying EOS is a mixture of different components, the entropy derived from Eq. (A5) implicitly includes the mixing terms, for instance the ideal entropy of mixing if the EOS is an ideal mixture. The constant of integration s_0 may depend on composition, but not on the initial condition of the planetary adiabat. If a mixture is kept constant during a planet's evolution, the offsets s_0 of planetary adiabats through different outer boundaries cancel each other, so that the real entropy difference between two adiabats is then known.

MOMENT OF INERTIA

The moment of inertia I of a rigid body with spin-angular velocity ω and axis of rotation \vec{e}_ω through the body's center of mass is

$$I = \int_V d^3r \rho(\vec{r}) (\vec{e}_\omega \times \vec{r})^2, \quad (\text{B1})$$

where the integral is taken over the volume V of the body. If we choose the orientation of the body such that \vec{e}_ω runs along the z -axis, then $(\vec{e}_\omega \times \vec{r})^2 = r^2 \sin^2 \vartheta$ in spherical coordinates. Because for an isolated fluid planet the assumption of hydrostatic equilibrium implies symmetry around the axis of rotation, Eq. (B1) becomes

$$I = 2\pi \int_0^\pi d\vartheta \int_0^R dr \rho(r, \vartheta) r^4 \sin^3 \vartheta, \quad (\text{B2})$$

where R is the planet's radius. If the planet rotates rapidly such as Jupiter, R depends on the latitude ϑ ; in particular, the equatorial radius $R_{\text{eq}} = R(\vartheta = \pi/2)$ is larger than the polar radius $R(\vartheta = 0)$. Therefore, in order to calculate the two-dimensional integral the figure of the planet must be known. The figure is the shape at an iso-bar surface, equivalently to an equipotential surface. For the solar system giant planets, this surface is taken to be the 1 bar pressure level by convention. We have used the *Theory of figures* (Zharkov & Trubitsyn 1978) to determine Jupiter's figure in terms of the figure functions $s_n(l)$ which give the shape of equipotential surfaces

$$r_l(l, \vartheta) = l \left(1 + \sum_{n=0}^{\infty} s_{2n}(l) P_{2n}(\cos \vartheta) \right). \quad (\text{B3})$$

If the new radial coordinate l is fixed, the total potential remains unchanged under variation of latitude ϑ . The functions $P_{2n}(\cos \vartheta)$ are the Legendre polynomials. Only even expansion coefficients occur because of the assumed symmetry between northern and southern hemisphere. The sum in Eq. (B3) is truncated after the third order term ($n = 3$) because that is sufficient to calculate the gravitational moment J_6 . We abbreviate the right hand side of the definition $r_l(l, \vartheta)$ by $r_l = l(1 + \sum)$. By inserting Eq. (B3) into Eq. (B2) and changing the independent variable from r to l using

$$dr/dl = \left[\left(1 + \sum s_{2n} P_{2n} \right) + l \left(\sum \frac{ds_{2n}}{dl} P_{2n} \right) \right], \quad (\text{B4})$$

and $l(P = 1 \text{ bar}) = R_m$, the mean radius, we can finally compute I ,

$$I = 2\pi \int_0^\pi d\vartheta \sin^3 \vartheta \int_0^{R_m} dl \left[(1 + \sum) + l \left(\sum \frac{ds_{2n}}{dl} P_{2n} \right) \right] \rho(l) l^4 (1 + \sum)^4. \quad (\text{B5})$$

In case of spherical symmetry, $\sum = 0$ and $ds_{2n}/dl = 0$.

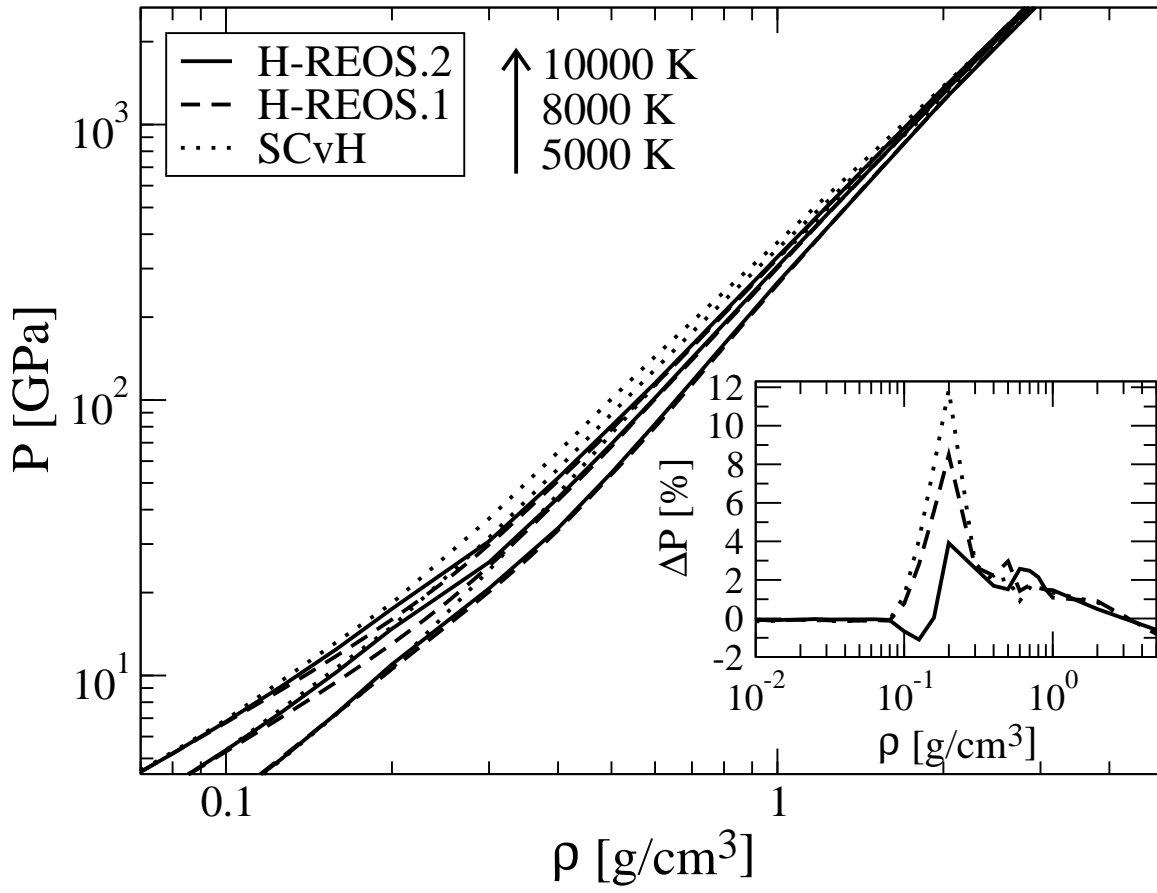


Figure 1. Hydrogen isotherms of different EOS; *solid*: H-REOS.2, *dashed*: H-REOS.1, and *dotted*: SCvH-i EOS. Inset: The relative deviation of H-REOS.2 with respect to H-REOS.1 for selected isotherms (5000 K: *solid*, 8000 K: *dotted*, 10000 K: *dashed*.)

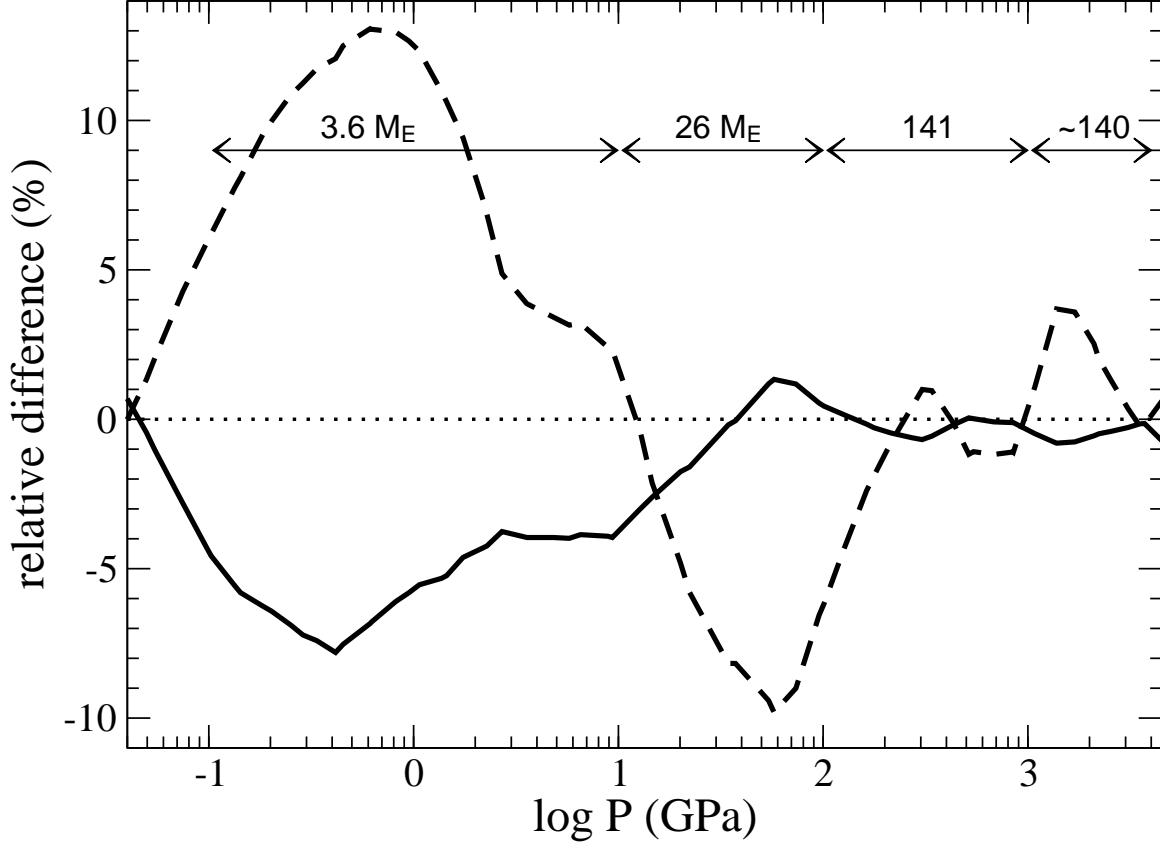


Figure 2. Relative difference in density (*solid*) and temperature (*dashed*) between the Jupiter adiabats calculated with H-REOS.1 and H-REOS.2, for a H-He mixture with $Y = 0.275$ (Jupiter average). The improved simulation of hydrogen dissociation causes systematically lower densities in the outer $\sim 16 M_{\oplus}$ of Jupiter. Numbers denote the mass in Earth masses between the pressure levels (in GPa) of 0.1-10, 10-100, 10-1000 as indicated by the arrows, and further up to 40 Mbar close to the core mantle boundary.

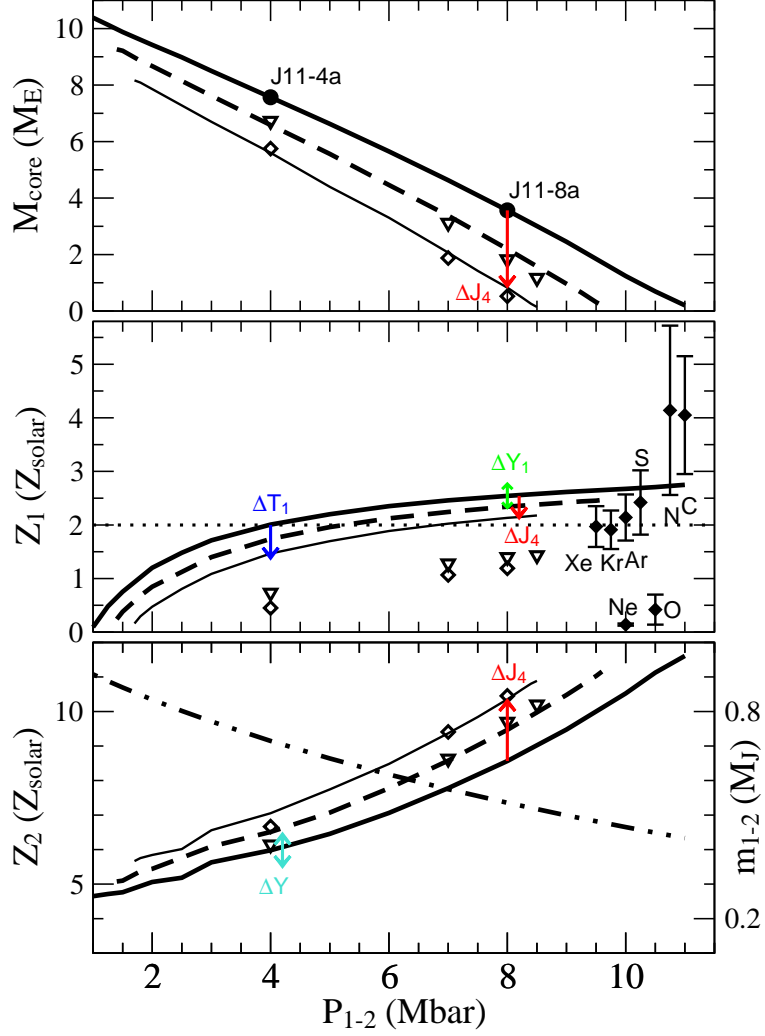


Figure 3. Jupiter interior models for different transition pressures P_{1-2} at the layer boundary. *Top:* core mass; *middle:* outer envelope metallicity scaled to the solar value $Z_{\text{solar}} = 0.015$; *bottom:* inner envelope metallicity. Curves are with the improved H EOS (H-REOS.2) and open symbols are models calculated with our former H-REOS.1. Among these, solid curves and triangles are for $J_4/10^{-4} = -5.89$, while dashed curves and diamonds are for $J_4/10^{-4} = -5.87$. The thick (thin) curves are calculated with the Theory of Figures to 3rd (4th) order. Arrows indicate the shift of the models J11-4a and J11-8a (filled circles) if the observational 1σ error bars of Y , Y_1 , T_1 , and J_4 are applied as described in § 3.1. Filled diamonds are measured atmospheric abundances in solar units placed arbitrarily on the x -axis. The dotted line is a guide to the eye for a (minimum) outer envelope metallicity of $2\times$ solar. The new models with H-REOS.2 are consistent with this constraint, but H-REOS.1 based models were not. The dot-dot-dash line in the bottom panel shows the scaled mass coordinate $m_{1-2} := m(P_{1-2})$, which is within the line thickness independent on the model assumptions. It can be used to calculate the mass of heavy elements in the envelopes $M_{Z,\text{env}} = Z_1 \times (M_J - m_{1-2}) + Z_2 \times (m_{1-2} - M_c)$.

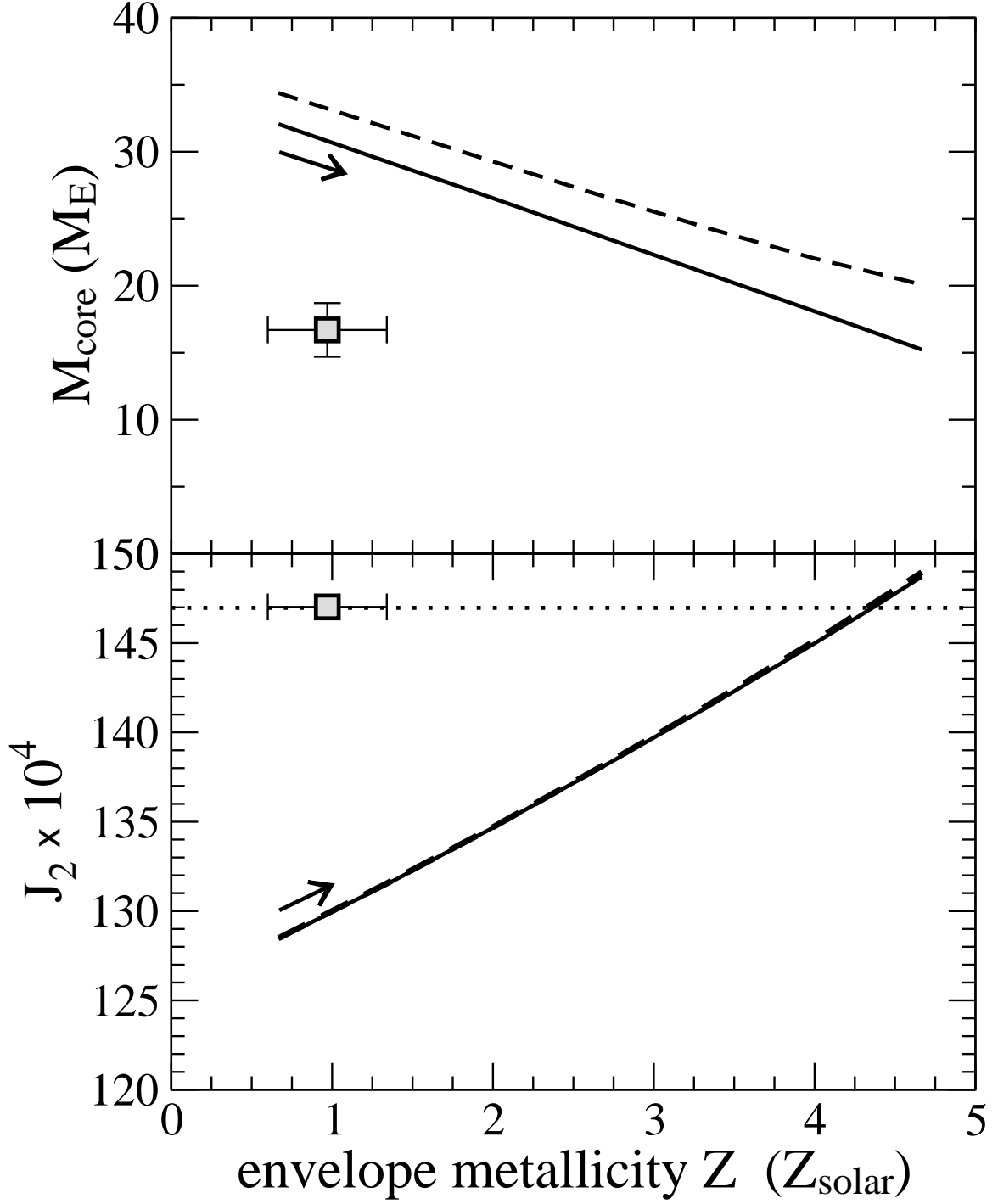


Figure 4. Two-layer models on their way to meet Jupiter's observed J_2 at 146.97×10^{-4} (vertical dotted line), starting at low envelope metallicity and moving in the direction as indicated by the arrows. The converged solution of our calculations is obtained through variation of Z . It has $Z = 4.33 Z_{\odot}$ and a core mass of $21.1 M_{\oplus}$ if the core is mostly ice (dashed), or $M_c = 16.5 M_{\oplus}$ if made of rocks (solid), respectively. Square with error bars: the M08 Jupiter model.

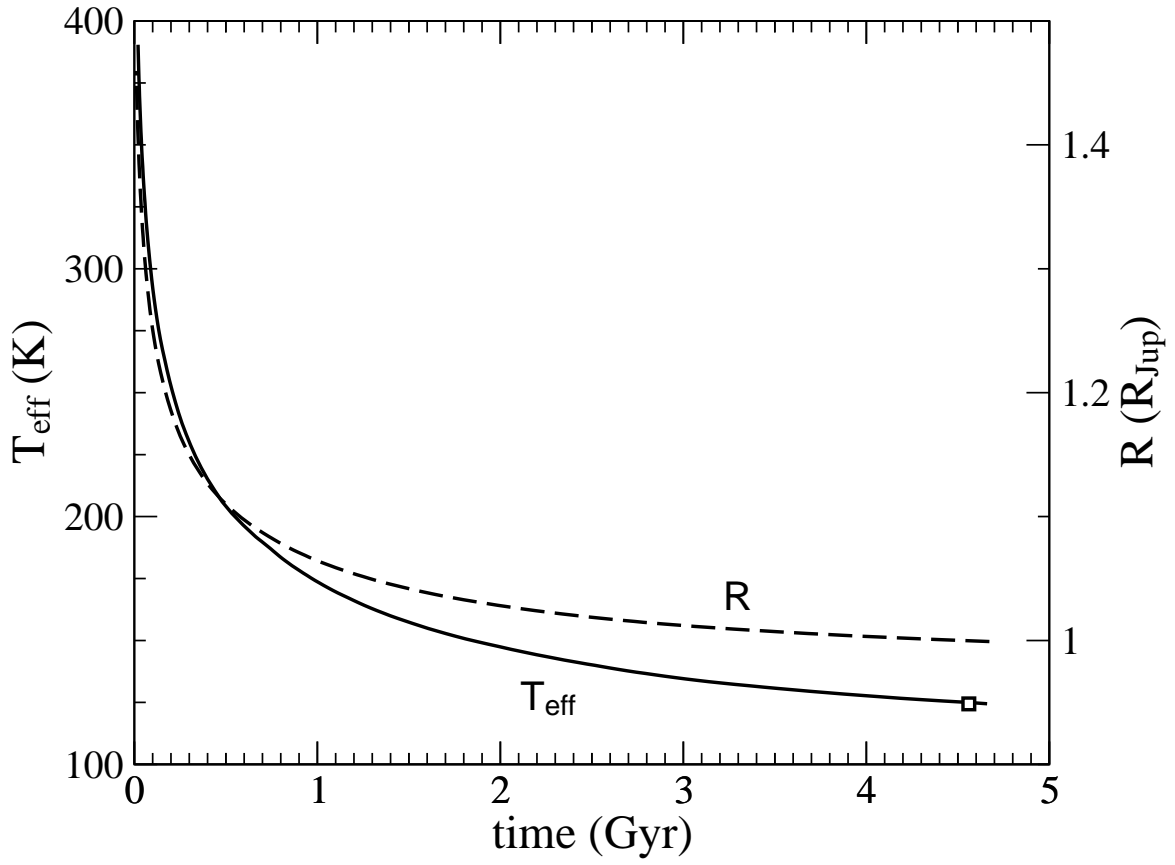


Figure 5. Effective temperature (*solid*) and mean radius (*dashed*) of the homogeneously cooling Jupiter (interior model J11-4a). The *square* indicates the observed T_{eff} at present time, whose observational error bar of 0.3 K is not resolved in this figure.

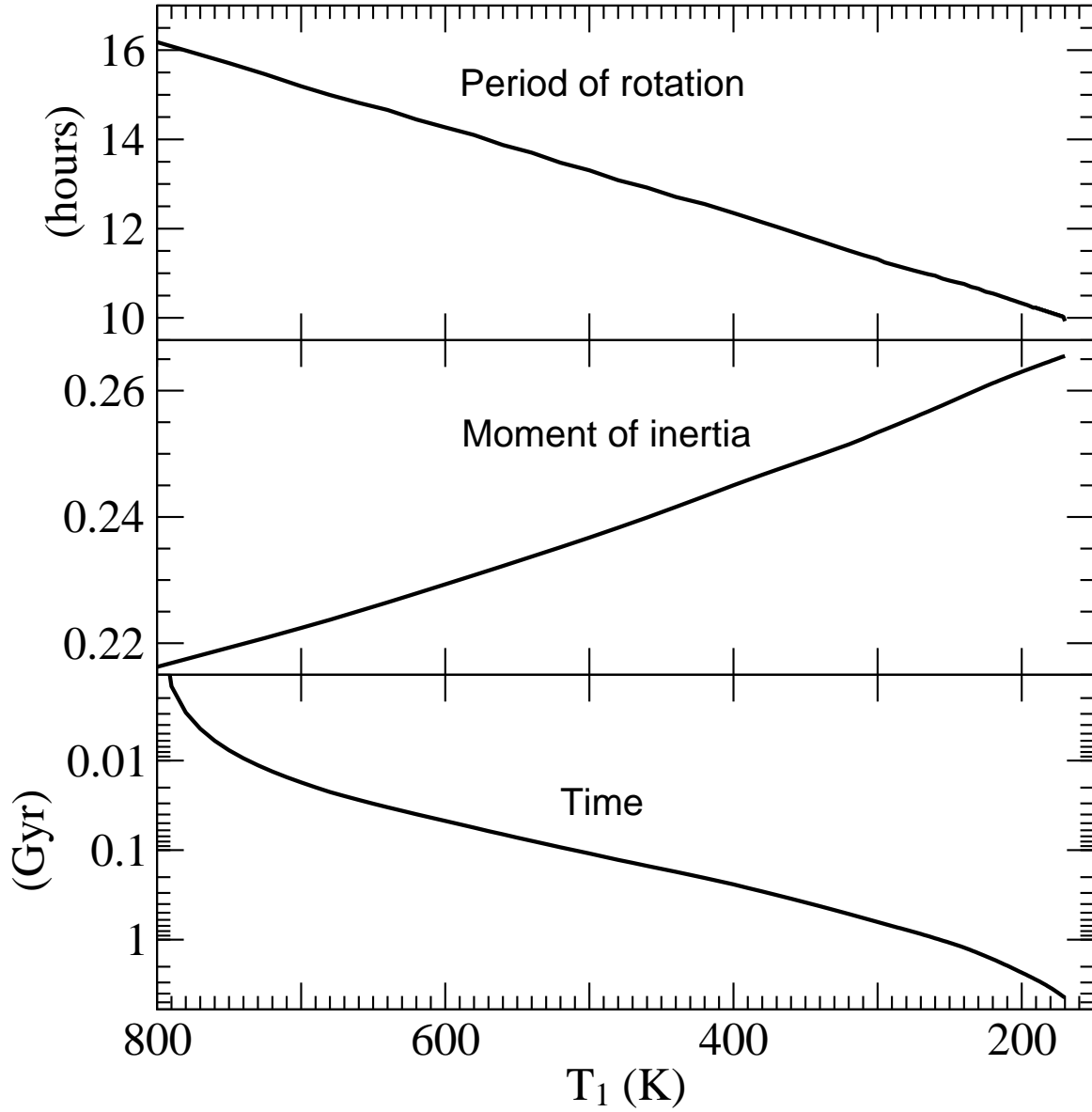


Figure 6. Jupiter’s evolution including angular momentum conservation, the corresponding change in the energy of rotation, and solar irradiation that increases with time. *Upper panel:* period of rotation; *middle panel:* normalized moment of inertia λ for the surface temperatures $T_1 = 170\text{--}800$ K that define the internal structure during the evolution. *Lower panel:* Map of T_1 onto time.

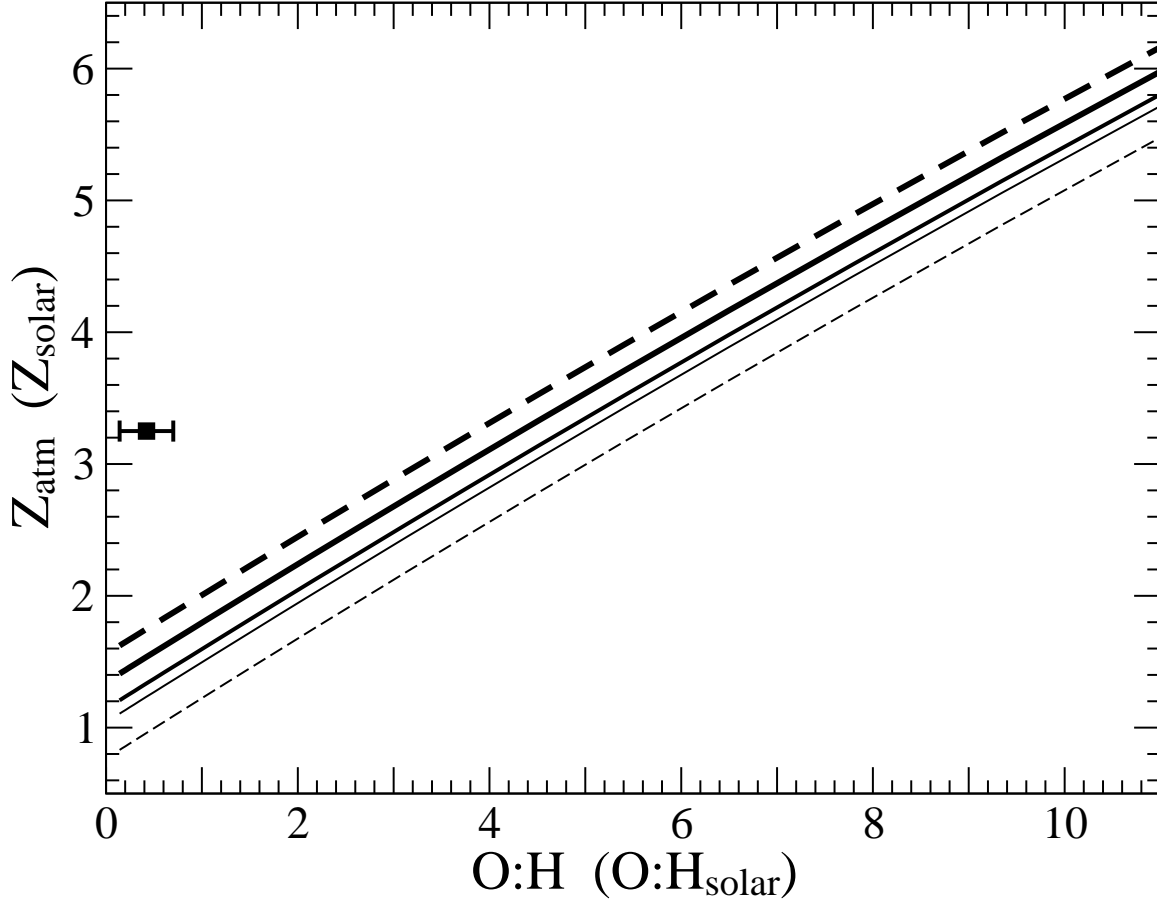


Figure 7. Metallicity Z_{atm} in Jupiter's deep atmosphere and outer envelope in dependence on the O:H ratio in solar units (Lodders 2003). *Thin solid*: using the mean values of the measured species (C,N,S,P,Ne,Ar,Xe,Kr); *solid (thick solid)*: including in addition $1\times$ ($3\times$) solar abundances of (Mg,Al,Ca); *thick dashed*: same as thick solid but using the upper limits of the measured abundances; *thin dashed*: same as thin solid but using the lower limits. The measured O:H abundance at 19 bars (Atreya et al. 2003) is indicated (vertical position has no meaning).

Table 1
Jupiter model J11-4a.

| m (M_{\oplus}) | P (GPa) | l (R_{m}) | T (K) | ρ (g cm^{-3}) | s_2 | s_4 | s_6 |
|-------------------------|--------------|---------------------------|------------|----------------------------------|--------------|-------------|--------------|
| 317.833802 | 1.0000E-04 | 1.000000 | 170.0 | 1.6970E-04 | -4.49641E-02 | 1.98582E-03 | -1.01995E-04 |
| ⋮ | ⋮ | ⋮ | ⋮ | ⋮ | ⋮ | ⋮ | ⋮ |
| 227.158225 | 3.9999E+02 | 0.735537 | 8995.9 | 1.3253E+00 | -3.53291E-02 | 1.09438E-03 | -3.82050E-05 |
| 227.155808 | 4.0001E+02 | 0.735532 | 8996.0 | 1.4332E+00 | -3.53290E-02 | 1.09437E-03 | -3.82046E-05 |
| ⋮ | ⋮ | ⋮ | ⋮ | ⋮ | ⋮ | ⋮ | ⋮ |
| 7.567754 | 4.2729E+03 | 0.114019 | 20041.2 | 4.3140E+00 | -1.00806E-02 | 8.05449E-05 | -6.72388E-07 |
| 7.567666 | 4.2729E+03 | 0.114018 | 20041.2 | 1.8815E+01 | -1.00805E-02 | 8.05447E-05 | -6.72385E-07 |

Note. — This table is published in its entirety in the electronic edition of the ApJ. A portion is shown here for guidance regarding its form and content. The columns show the internal profile of the Jupiter model J11-4a in terms of the mass coordinate m , the pressure P , the radial coordinate l scaled by Jupiter’s calculated mean radius $R_{\text{m}} = 10.95517R_{\oplus}$, the temperature T , the density ρ , and the figure functions s_2 – s_6 , see Appendix B.